Detectability of Changes in the Walker Circulation in Response to Global Warming

Pedro N. DiNezio

International Pacific Research Center, School of Ocean and Earth Science and Technology, University of Hawaii, Honolulu, Hawaii

Gabriel A. Vecchi

NOAA/Geophysical Fluid Dynamics Laboratory, Princeton, New Jersey

Amy C. Clement

Rosenstiel School of Marine and Atmospheric Science, University of Miami, Miami, Florida

Submitted to J. Climate

Corresponding author address: Pedro N. DiNezio,

E-mail: pdn@hawaii.edu International Pacific Research Center, School of Ocean and Earth Science and Technology, University of Hawaii, Honolulu, Hawaii 96822

Abstract

Changes in the gradients in sea level pressure (SLP) and sea surface temperature (SST) along the equatorial Pacific are analyzed in observations and 101 numerical experiments performed with 37 climate models participating the Fifth Phase of the Coupled Model Intercomparison Project (CMIP5). The ensemble of numerical experiments simulates changes in the Earth's climate during the 1870-2004 period in response to changes in natural (solar variations, volcanoes) and anthropogenic (well-mixed greenhouse gases, ozone, direct aerosol forcing and land use) radiative forcings. A reduction in the zonal SLP gradient is present in observational records, and is the typical response of the ensemble; yet only four of these experiments are able to simulate the magnitude of the observed weakening of the SLP gradient during the 1870-2004 period. The multi-model response indicates a reduction of the Walker circulation to past forcing of between 50% and 33% of the observed trend. There are multiple, non-exclusive interpretations of these results: i) the observed trend may not be entirely forced, and includes a substantial component from internal variability, and/or ii) there are problems with the observational record that lead to a spuriously large trend. iii) the strength of the Walker circulation, as measured by the zonal SLP gradient, may be less sensitive to external forcing in models than in the real climate system. Analysis of a subset of experiments suggests that greenhouse gases act to weaken the circulation, but aerosol forcing drives a strengthening of the circulation, which appears to be overestimated by the models, resulting in a muted response to the combined anthropogenic forcings.

Introduction

Observations exhibit a reduction in the east-west contrast in sea level pressure (SLP) along the equatorial Pacific during the 20th Century (Vecchi *et al.* 2006; Zhang *et al.* 2006; Power and Smith 2007; Karnauskas *et al.* 2009; DiNezio *et al.* 2010) (Figure 1). This trend reflects a weakening of the Walker circulation – the large-scale zonal flow of air with convective motion over the Maritime continent and subsidence over the central and eastern Pacific Ocean. This weakening of the Walker circulation was first attributed by Vecchi *et al.* (2006; V06) using an ensemble of 3 numerical experiments performed with the GFDL-CM2.1 model. The spatial pattern and magnitude of the SLP trends observed over the tropical Indo-Pacific during 1861-1992 agree with the simulated changes, only when the model is forced with anthropogenic changes in radiative forcings. This response is also a robust feature of global warming simulations for the 21st Century, where the ascending branch of the Walker circulation weakens in order to maintain a balanced transport of water vapor in areas of convection, as precipitation increases in response to surface warming at a smaller rate than humidity (Held and Soden 2006; Vecchi and Soden 2007). This differential in the rates of change of humidity and precipitation has not been detected in observations, though the length and quality of the observational record may be insufficient to constrain the response of global precipitation (Chou and Neelin 2004; Wentz *et al.* 2007; Liepert and Previdi 2009).

The detection and attribution of the forced weakening of the Walker circulation can be confounded by the very large *internal* variability of the tropical Pacific (V06; Deser *et al.* 2010b; Power and Kociuba 2011). For instance, the observed SLP trends

72 exhibit a large reversal since the 1990s with stronger trade winds and Walker circulation
73 (Merrifield 2011). Conversely, the largest multi-decadal weakening of the Walker
74 circulation occurred during the 1977–2006 period coincident with an increase in the
75 frequency of El Nino and a reduction in the frequency of La Nina (Power and Smith
76 2007). Previous studies have estimated a wide range of detection time scales from 60
77 years (Tokinaga *et al.* 2012) to 130 years (V06).

78 Are natural internally generated changes in the Walker circulation masking the
79 forced signal due to global warming? Model sensitivity to warming and the magnitude of
80 the internal variability differ from model to model, thus the detectability of the forced
81 changes is likely to be model dependent. In order to overcome this issue, Power and
82 Kociuba (2011) analyzed SLP trends simulated by a multi-model ensemble of
83 simulations of the 20th Century climate coordinated by the Coupled Model
84 Intercomparison Project phase 3 (CMIP3). Their results suggest that the observed SLP
85 trends during the twentieth century are due to a combination of both unforced internal
86 climate variability and GHG-forced global warming.

87 Here we address these questions comparing trends in SLP and SST observations
88 with 101 "historical" experiments performed with 37 climate models participating in the
89 Fifth Phase of the Coupled Model Intercomparison Project (CMIP5). Note that the
90 attribution study done by V06 relied on an ensemble of 5 simulations using one single
91 model, GFDL-CM2.1. Deser *et al.* (2010b) used the CCSM3.0 model to show that
92 ensembles of at least 20 simulations are required to isolate forced changes in tropical
93 circulation in response to 21st Century forcings. Power and Kociuba (2011) used a multi-
94 model ensemble of 20th Century climate simulations coordinated by 3rd Phase of the

Coupled Model Intercomparison Project (CMIP3). Here we apply their methodology to a much larger ensemble of 20th Century climate simulations coordinated by CMIP5. We look at each model's range of simulated changes in order to determine whether the forced weakening of the Walker circulation is already detectable in the modern observational record. To conclude we use a subset of new CMIP5 experiments, where the models are forced solely with each type of forcing, to explore how the different anthropogenic and natural forcings could drive changes in the Walker circulation.

Model and Observational Data

We use observed and simulated SLP and SST data to detect and attribute changes in the strength of the Walker circulation during the 1870-2004 period and its relationship with patterns of warming. The observed data are monthly mean SLP fields from the HadSLP2 dataset (Allan and Ansell 2006) and monthly mean SST fields from the ERSST3 (Smith *et al.* 2008) and HadISST (Rayner *et al.* 2003) datasets. The simulated data consists of monthly mean SLP and SST fields from an ensemble of 104 'historical' experiments coordinated by CMIP5 and performed with 37 different coupled climate models. These 'historical' experiments simulate changes in the Earth's climate during the 1850-2005 period in response to changes in natural (solar variations, volcanoes) and anthropogenic (well-mixed greenhouse gases, ozone, direct aerosol forcing and land use) radiative forcings. We also use an ensemble of 31 historical experiments performed with 7 different models forced solely with GHG or natural forcing (historicalGHG and historicalNat in the CMIP5 archive) to explore the origin of the SLP trends.

We estimate the variability and change in the east-west SLP gradient along the equatorial Pacific ocean both from observations and each simulation. For this we use the dSLP index defined by V06 as the difference of the area averaged SLP between a "Tahiti" region (160°W–80°W, 5°S–5°N) minus a "Darwin" region (100°E–180°, 5°S–5°N). This index measures changes in the zonal SLP gradient along the equatorial Pacific a proxy for the strength of the Walker circulation. We also define a dSST index as the difference of the area averaged SST between the Tahiti and Darwin regions to explore the relationship between changes in the SST gradient and the Walker circulation.

Most CMIP5 historical experiments begin in 1850, and a few others in 1860. The HadISST and ERSST3 datasets start in 1870 and the HadSLP2 record in 1860. All observational datasets extend until 2004. There is a near-real time SLP dataset (HadSLP2r) that extends until 2012, but the variance in the HadSLP2r is larger after 2005 potentially introducing spurious trends (See next subsection). For these reasons we focus in the 1870-2004 period when all three observational datasets and historical simulations have coinciding data. The changes in the dSLP and dSST indices are computed as least-squares linear trends in each individual 'historical' experiment over the 1870 – 2004. We also explore the detectability of the trends during shorter periods beginning from 1870 to 1970, all ending in 2004.

a. Issues with SLP datasets after 2005

This study could be extended until 2012 using an extension of the historical experiment (historicalExt) or any of the emission scenario experiments (rcp45, rcp60, rcp85) coordinated by CMIP5, along with the HadSLP2r dataset for observed changes.

The HadSLP2r dataset is an extended HadSLP2 dataset in which SLP fields from the NCEP-NCAR reanalysis (Kalnay *et al.* 1996) are appended to the HadSLP2 dataset after 2004, to allow analyses to the present. The HadSLP2 dataset (Allan and Ansell 2006) is a spatially-complete dataset of SLP from 1860-2004, in which a consistent methodology was applied to sparse observations to generate global reconstructions of SLP, and therefore suitable for climate applications. The HadSLP2r is widely used for climate applications, even though it is a concatenation of two disparate datasets. After exploring the character of the HadSLP2r SLP evolution (Figure 2), we have decided against using it, since it includes a spurious shift in its variance characteristics that impacts trends and other estimates of multi-decadal to centennial change. The inhomogeneity of HadSLP2r across the 2004-2005 data splice is also likely to be problematic for many other applications – the lower panels in Figure 2 focus on the impact to near-Equatorial Pacific SLP, but comparable impacts are seen throughout the globe.

The "real time" extension of HadSLP2 is done by appending SLP values from the NCEP reanalysis to HadSLP2; the NCEP data is correlated only for the mean differences in SLP between HadSLP2 and NCEP over the overlapping period. However, HadSLP2 is a reconstruction from a sparse data network, a property of which is to reduce the variance of the overall anomalies - to recover a consistent reconstruction over the entire record. Meanwhile NCEP is a model-based reanalysis, which does not aim to reduce variance. Therefore, though the mean differences between the two products are corrected, differences in the variance are not. As can be seen in Figure 2, starting in 2005, the character of anomalies in HadSLP2r changes markedly. Therefore, HadSLP2r cannot be

160 treated as a climate data record to explore changes in the character of SLP across the
161 2004-2005 boundary.

162 Detection and Attribution of the Observed Changes

163 There is clear evidence from previous studies that the dSLP trends in each
164 individual experiment include both forced and unforced changes. Multi-decadal trends
165 due to unforced internal variability are likely to dominate the trends during periods
166 shorter than 100 yr (V06). We address these issues by computing the multi-model
167 ensemble-mean (MMEM) and the probability density function (PDF) of the dSLP trends
168 for a range of detections periods ending on 2004, but starting sequentially from 1870
169 every 10 years until 1980. Figure 3 shows the MMEM (solid white line) and the PDF
170 (colors) of the dSLP trends (y-axis) as a function of the start date of the detection period
171 (x-axis). The ensemble of 'historical' experiments analyzed here provides 101
172 independent realizations of climate that we use in the estimation of the MMEM and PDF
173 of the trends. Trends due to random unforced variability cancel out in the averaging,
174 resulting in a MMEM trend that estimates the magnitude of the forced trend. Conversely,
175 the PDF characterizes the possible trend values associated with differences in model
176 physics, as well as random internal variability. The PDFs for each detection period are
177 computed using the kernel density estimation method (Parzen 1962).

178 The MMEM dSLP trend has a magnitude of -0.05 ± 0.02 hPa / 100 yr during the
179 1870 – 2004 period, indicating a weakening of the SLP gradient (Figure 3, white line).
180 The error of the MMEM dSLP is the standard error of 101 simulated dSLP trends. The

181 magnitude of this weakening increases slowly for shorter detection periods, reaching a
182 value of -0.13 ± 0.05 hPa / 100 yr for the 1960 – 2004 period. Conversely, The PDF of
183 the dSLP trends widens as the detection period shortens (Figure 3, shading). However,
184 even for the 1870-2004 detection period, a substantial fraction of the trends (25%) are
185 positive, indicating that the Walker circulation strengthens in these models. The PDF of
186 the dSLP trends becomes nearly uniform for detection periods beginning in 1970. This
187 indicates that a wide range of positive or negative trends are equally likely, despite the
188 fact that the MMEM trend, *i.e.,* the forced trend, is non-zero. For longer detection periods
189 beginning from 1870 to 1950 the spread of the simulated dSLP trends appears to be
190 dominated by inter-model differences in the magnitude of the forced response, with
191 internal variability playing a lesser role. We interpret the difference of the PDF for longer
192 and shorter detection periods to be because the more recent trends are dominated by
193 unforced, *i.e.* random, multi-decadal internal variability.

194 In contrast, the magnitude of the observed dSLP trend during the 1870 – 2004
195 period is 0.42 ± 0.14 hPa / 100 yr. Similar trend values are obtained from detection
196 periods starting in 1870 through 1920. The magnitude of the observed dSLP trend is not
197 only much larger than the MMEM value of -0.05 ± 0.18 hPa / 100 yr (Figure 3, black
198 line), but also very unlikely to occur in response to changes in forcing, according to the
199 multi-model PDF. In fact, there are only five experiments (out of 101) that simulate dSLP
200 trends within the 1σ confidence limits of the observed dSLP trend.

201 What is the contribution of forced and unforced variability to the observed trend?
202 In order to answer this question we compute the ensemble mean (EM) dSLP and dSST
203 trends for those models with more than one historical 'experiment'. We also expect that

each model's EM will capture the magnitude of the forced trend. In this analysis we include the dSST trends in order to explore the role of patterns in warming in the response of the Walker circulation. Note that none of the models has run up to 20 ensemble members required to isolate forced trends (Deser *et al.* 2010b). Thus, we also estimate the range of trends simulated by each model in the different experiments as an estimate of the uncertainty due to internal variability.

A total of 12 models simulate EM dSLP trends that are negative over the 1870-2004 period (Figure 4a, red dots, y-axis). However, some of the individual experiments simulate positive dSLP trends, despite the fact that respective EM trends are negative (e.g. CNRM-CM5, CSIRO-Mk3-6-0, CanESM2, IPSL-CM5A-LR, HadGEM2-ES). These models suggest that unforced century-timescale trends can overwhelm the forced signals. Only five models (CanESM2, GISS-E2-R, MIROC-ESM, MPI-ESM-LR, MRI-CGCM3) simulate a detectable weakening of the Walker circulation, i.e. all the experiments performed with these models simulate negative dSLP trends (Figure 4, dots 9, 13 and 5).

Because of the strong coupling between equatorial SST and SLP gradients (Bjerknes 1969), one would expect that models with a weaker Walker circulation would simulate a weaker SST gradient. However, not all the models that simulate a weakening of the Walker circulation (EM dSLP trend < 0) simulate a weakened east-west sea surface temperature gradient (EM dSST trend < 0) (Figure 4, red dots, x-axis). This could occur because the weakening of the Walker circulation is driven by changes in the hydrological cycle driving that are governed by the magnitude of tropical mean warming, even in the absence of patterns of warming. Conversely, the boxes used to compute dSST might not be optimally located to capture the changes that are relevant for each particular model.

227 We explored several definitions of the zonal SST gradient, and none of them show a clear
228 relationship with the SLP gradient.

229 In general, however, the changes in dSST seem to play a role because the models
230 with weaker dSST simulate the largest weakening in dSLP (e.g. MIROC-ESM).
231 Conversely, the models that simulate stronger Walker circulations tend to simulate a
232 stronger SST gradient (dSST trend > 0) (e.g. GFDL-CM3). An alternative explanation is
233 that even for periods as long as 1870-2004, the individual trends could be dominated by
234 internal variability in the tropical Pacific, which exhibits highly correlated changes in
235 SLP and SST gradients since it arises from coupled ocean-atmosphere interactions. The
236 high correlation ($r = 0.81$) between the dSLP and dSST trends of the individual
237 experiments (Figure 4, gray dots) supports this idea. The trends in ERSST3 agree well
238 with the experiments with the largest dSLP and dSST trends (MIROC-ESM and MRI-
239 CGCM3). In contrast, there is no experiment that simulates dSST and dSLP trends
240 comparable to those than HadISST and HadSLP2.

241 Only four experiments simulate dSLP trends with a magnitude comparable to the
242 observed values. Two of these experiments were performed with MIROC-ESM, which is
243 the only model that simulates an EM dSLP comparable with the observed value, thus
244 according to this model, the observed trends would be entirely forced. Note that despite
245 only 3 realizations were used to compute the EM trend, the weaker internal variability
246 simulated by this model allows the forced response to dominate in all the experiments.
247 One of the remaining two experiments was performed with MRI-CGCM3 (experiment
248 r5i1p1), which exhibits a dSLP trend of -0.30 hPa / 100 yr. Note that the EM trend of
249 MRI-CGCM3 is -0.15 hPa / 100 yr, thus, according to this model, the observed trend is

about equal parts forced and unforced. The remaining experiment was performed with CSIRO-Mk3-6-0 (experiment r6i1p1) and shows a dSLP trend of -0.28 hPa / 100 yr. This model's EM dSLP trend is -0.09 hPa / 100 yr, thus according to this model, the observed trend is 2/3 due to internal variability and 1/3 due to a forced response. The observed dSLP trend during 1870-2004 is often attributed to the very strong 1982 and 1997 El Nino events at the end of the record. However, the -0.42 ± 0.14 hPa / 100 yr trend during the entire 1870-2004 period (Figure 1, magenta line), is not statistically different from the -0.33 ± 0.18 hPa / 100 yr trend during the 1870-1980 period, which excludes these large El Nino events (Figure 1, magenta line).

a. Sensitivity to Historical Forcings

The smaller-than-observed sensitivity of the Walker circulation to historical forcing exhibited by the CMIP5 models may also have resulted from opposing responses to the natural and anthropogenic forcings included in the 'historical' experiment. Analysis of historicalGHG experiments performed with a smaller set of models shows evidence for this explanation. Five out of seven models show a larger response in the dSLP gradient when forced solely by changes in GHG gases (Figure 5). Note that the number of ensemble members may not be large enough to isolate the responses to the different forcing. However, the experiments performed with GFDL-CM3, GISS-E2-H, GISS-E2-R CCSM4 exhibit dSLP trends in response to GHG-only forcing (Figure 5, blue bars) that fall outside the min-max range of trends simulated in response to all forcings (Figure 5, blue bars) or to natural forcings (Figure 5, green).

The impact of each forcing on the changes in the Walker circulation is clearly shown by the shifts in the PDFs of the 1970-2004 dSLP trends (Figure 6a). The PDF of the historicalNat experiments shows no tendency for changes in dSLP (green), while the the PDF of the historicalGHG experiments shows a stronger sensitivity than to all historical forcing (natural and anthropogenic) combined (blue). The fact that the weakening of the Walker circulation to all historical forcing changes is smaller than to only GHG increases suggests that the anthropogenic aerosols, which are only included in the 'all forcing' experiments, are acting to strengthen the circulation. The enhanced sensitivity to GHG forcing, however, does not prevent internal variability from overwhelming the forced trends on shorter periods, such as 1970-2004 (Figure 6b), when 33% of the historicalGHG experiments still exhibit positive trends.

Discussion and Conclusions

Analysis of 101 simulations of the climate of the 1870-2004 period coordinated by CMIP5 shows that the Walker circulation appears to be less sensitive to external forcing in models than in observations. The magnitude of the observed weakening agrees with the EM response in only one model (MIROC-ESM). Alternatively, two experiments performed with MRI-CGCM3 and CSIRO-Mk3-6-0 simulate trends that agree (within 1σ statistical confidence) with the observed value of -0.45 hPa / 100 yr. In these experiments the trends are due to a combination of forced and internal variability. Therefore the observed trend may not be entirely forced, and the true sensitivity of the Walker

291 circulation could be between 50% and 33% of the observed trend in agreement with a
292 previous study based on the CMIP3 archive (Power and Kociuba 2011).

293 The fact that the observed trend can only be explained by 4 out of 101
294 experiments could be pointing to issues in the models or the observations. The observed
295 trend could be the result of spurious trends or biases, especially over ocean regions such
296 as our equatorial "Tahiti" box, which have low data density before the 1940s (Allan and
297 Ansell 2006). However, the 1877-2005 trend in SLP gradient has been estimated using
298 data solely from the "Darwin" box, where coverage is more stable in time (Bunge and
299 Clarke 2009). This method yields a 1977-2005 trend of -0.45 hPa / 100 yr, which is
300 virtually identical to the trend estimated from HadSLP2. Therefore the discrepancy
301 between the model ensemble and observations could indicate that the Walker circulation
302 in the models is not as sensitive to anthropogenic forcings as that in the real climate
303 system. This conjecture is supported by a subset of models that show a weakening of the
304 Walker circulation in response to GHG forcing closer to the observed value, but which
305 appears to be opposed by forcing by anthropogenic aerosols. We are currently exploring
306 this issue with a more detailed experimental approach due to its relevance for attributing
307 not only the observed centennial-scale trend, but also the recent strengthening trend that
308 has occurred in coincidence with the increase in aerosol forcing from Asia.

309 Evidence for a weaker Walker circulation is usually sought in the changes in the
310 zonal SST gradient, because of the close relationship between dSLP and dSST on
311 interannual and decadal timescales. However, the models do not show a reduction in
312 dSST as robust as the weaker dSLP. We suggest that this is because the weakening of the
313 Walker circulation is driven by changes in the hydrological cycle that are not related to

changes in the SST gradient, but to the magnitude of tropical mean warming (Held and Soden 2006; Vecchi and Soden 2007; DiNezio *et al*. 2010). Moreover, the different observational SST datasets show conflicting trends already reported by previous studies (Vecchi *et al.* 2008; Deser *et al.* 2010a). Poor data coverage in the equatorial Pacific makes it difficult to accurately estimate dSST (*Deser et al.* 2010a). The decadal signals and trend in ERSST3 dataset show the best agreement with a verified estimation of the Nino3.4 index (Bunge and Clarke 2009). Moreover, the trends in ERSST3 agree well with the experiments with the largest dSLP and dSST trends (MIROC-ESM and MRI-CGCM3). This suggests that weakened SST gradients may play a role in a weakening of the SLP gradient with the observed magnitude.

Beginning in 1920 the observed trends show multi-decadal variations, weakening down to -0.8 hPa / 100 yr during 1950-2004, even with a shift to positive trends, i.e. stronger Walker circulation, for trends beginning in 1970 (1.7 hPa / 100 yr during 1980-2004) These trends are much different from the long-term trends of about 0.4 hPa / 100 yr computed from initial dates ranging from 1870 to 1920, thus are likely to result from the multi-decadal internal variability. Models also simulate a wide range of possible trends for detection periods beginning after the 1920s, thus confirming the results of V06 that records longer than 100 years are required to detect changes in the Walker circulation. According to the models it is very likely that changes detected in the tropical Pacific during the last 60 years (*e.g.*, Merrifield 2011; Tokinaga *et al.* 2012) will be dominated by internal variability, reducing our ability to detect and attribute a forced trend in the recent part of the observation record.

Acknowledgements

We acknowledge the World Climate Research Programme's Working Group on Coupled Modelling, which is responsible for CMIP, and we thank the climate modeling groups for producing and making available their model output. For CMIP the U.S. Department of Energy's Program for Climate Model Diagnosis and Intercomparison provides coordinating support and led development of software infrastructure in partnership with the Global Organization for Earth System Science Portals. P. N. DiNezio was supported by NSF (grant AGS 1203754) and the University of Hawaii. AC was supported by NSF (AGS0946225), NOAA (NA10OAR4310204), and DOE (DESC0004897).

References

Allan, R., and T. Ansell, 2006: A New Globally Complete Monthly Historical Gridded Mean Sea Level Pressure Dataset (HadSLP2): 1850–2004. *J. Climate*, **19**, 5816–5842.

Bunge, L., and A. J. Clarke, 2009: A verified estimation of the El Niño index NINO3.4 since 1877, *J. Climate*, **22**, 3979–3992.

Chou, C., and J. D. Neelin, 2004: Mechanisms of global warming impacts on regional tropical precipitation. *J. Climate*, **17**, 2688-2701.

Deser C., A. Phillips, and M. A. Alexander, 2010a: Twentieth century tropical sea surface temperature trends revisited. *Geophys. Res. Lett.*, **37**, L10701, doi:10.1029/2010GL043321.

Deser, C., A. S. Phillips, V. Bourdette, and H. Teng, 2010b: Uncertainty in climate change projections: The role of internal variability. *Clim. Dyn.*, **38**, 527-546, DOI 10.1007/s00382-010-0977-x.

DiNezio, P.N., A.C. Clement, and G.A. Vecchi, 2010: Reconciling Differing Views of Tropical Pacific Climate Change. *Eos, Trans. AGU*, **91** (16), 141-142.

Kalnay, E., M. and coauthors, 1996: The NCEP/NCAR 40-year reanalysis project, *Bull. Amer. Meteor. Soc.,* **77**(3), 437–470.

Karnauskas, K.B., R. Seager, A. Kaplan, Y. Kushnir, and M.A. Cane, 2009: Observed strengthening of the zonal sea surface temperature gradient across the equatorial Pacific Ocean. *J. Climate*, **22**(16), 4316–4321.

368 Merrifield, M. A., 2011: A shift in western tropical Pacific sea level trends during the
369 1990s, *J. Climate*, **24**, 4126–4138.

370 Parzen, E., 1962: On estimation of a probability density function and mode, Annals of
371 Mathematical Statistics, **33**, 1065–1076, DOI:10.1214/aoms/1177704472.

372 Power, S. B., and G. Kociuba, 2011: What Caused the Observed Twentieth-Century
373 Weakening of the Walker Circulation? *J. Climate*, **24**, 6501–6514.

374 Rayner, N. A., and Coauthors, 2003: Global analyses of sea surface temperature, sea ice,
375 and night marine air temperature since the late nineteenth century. *J. Geophys.*
376 *Res.*, **108**, 4407.

377 Smith, T. M., R. W. Reynolds, T. C. Peterson, and J. Lawrimore, 2008: Improvements to
378 NOAA's Historical Merged Land-Ocean Surface Temperature Analysis (1880-
379 2006). *J. Climate*, **21**, 2283–2296.

380 Tokinaga, H., S.-P. Xie, A. Timmermann, S. McGregor, T. Ogata, H. Kubota, and Y. M.
381 Okumura, 2012: Regional Patterns of Tropical Indo-Pacific Climate Change:
382 Evidence of the Walker Circulation Weakening. J. Climate, **25**, 1689-1710.

383 Vecchi, G. A., B. J. Soden, A. T. Wittenberg, I. M. Held, A. Leetmaa, and M. J. Harrison,
384 2006: Weakening of tropical Pacific atmospheric circulation due to anthropogenic
385 forcing. *Nature*. **441**, doi:10.1038/nature04744.

386 Vecchi, G. A., and B. J. Soden, 2007a: Global Warming and the weakening of the
387 tropical. circulation, *J. Climate*, **20**, 4316–4340.

388 Vecchi, G. A., A. Clement, and B. J. Soden, 2008: Examining the tropical pacific's
389 response to global warming. *EOS, Trans AGU*, **89**(9), 8183.

390 Wentz, F. J., L. Ricciardulli, K. Hilburn, and C. Mears, 2007: How much more rain will
391 global warming bring? *Science*, **317**, 233–235.
392 Zhang, M., and H. Song, 2006: Evidence of deceleration of atmospheric vertical
393 overturning circulation over the tropical Pacific. *Geophys. Res. Lett.*, **33**, L12701.
394

Table of Figures

that the shaded area covers 99%, 95%, and 66% of the trends respectively. See Figure 1 or Section 2 for details on the computation of dSLP index. The detection periods begin at different years from 1870 to 1980 (x-axis) all ending in 2004. The solid white line is the multi-model ensemble-mean trend dSLP trends for each detection period. The solid black line is the observed trend for each detection period. The thin black lines delimit the 1σ confidence interval of the observed trends computed from Student-t distribution with reduced degrees of freedom accounting for auto-correlation in the dSLP index. 25

Figure 4 – Linear trends in the east-west equatorial gradients of sea surface temperature (dSST) and sea level pressure (dSLP) during the 1870 to 2004 period in observations (blue) and in CMIP5 historical experiments (red). The SLP gradient (dSLP) is a measure of the strength of the Walker circulation. See Figure 1 or Section 2 for details on the dSLP and dSST indeces. The red dots are the ensemble-mean trend for each model and the error bars show the spread among the trends simulated by the model in each experiment. The error bars are the max-min values of the dSLP and dSST trends. The gray dots are the trends from each individual experiment. Only changes simulated by models with more than one historical experiment are shown. The number along with the model name indicates the number of runs of the historical experiment run by each model. The error bars of the observed trends is given by the 1σ confidence interval computed using a Student-t with reduced degrees of freedom to account for auto-correlation in the timeseries. 26

Figure 5 – Linear trends in the east-west sea level pressure gradient (dSLP) during the 1870 to 2004 period simulated by CMIP5 historical (blue), historicalGHG (red), and

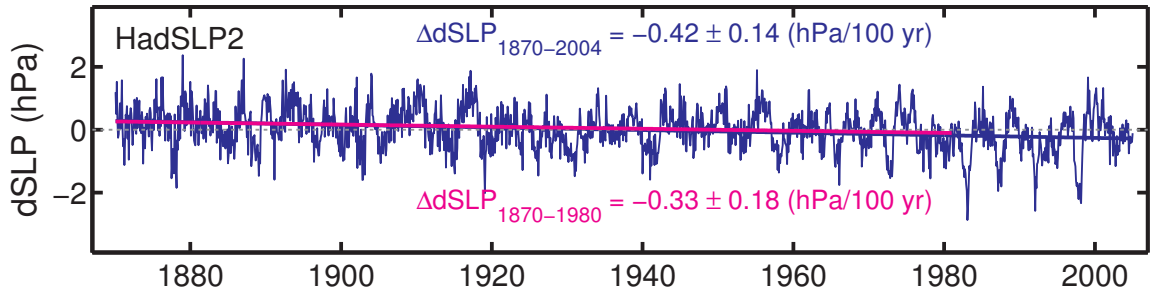

Figure 1 – Observed time series of zonal equatorial gradient in sea level pressure (dSLP) during the 1870 to 2004 period (HadSLP2 dataset). The SLP gradient (dSLP) is a measure of the strength of the Walker circulation. The dSLP timeseries is computed as the area-average of the monthly SLP fields over a "Tahiti" region (160°W–80°W, 5°S–5°N) minus a "Darwin" region (100°E–180°, 5°S–5°N). The error bar of the trends are given by the 1σ confidence interval computed using a Student-t with reduced degrees of freedom to account for auto-correlation in the timeseries.

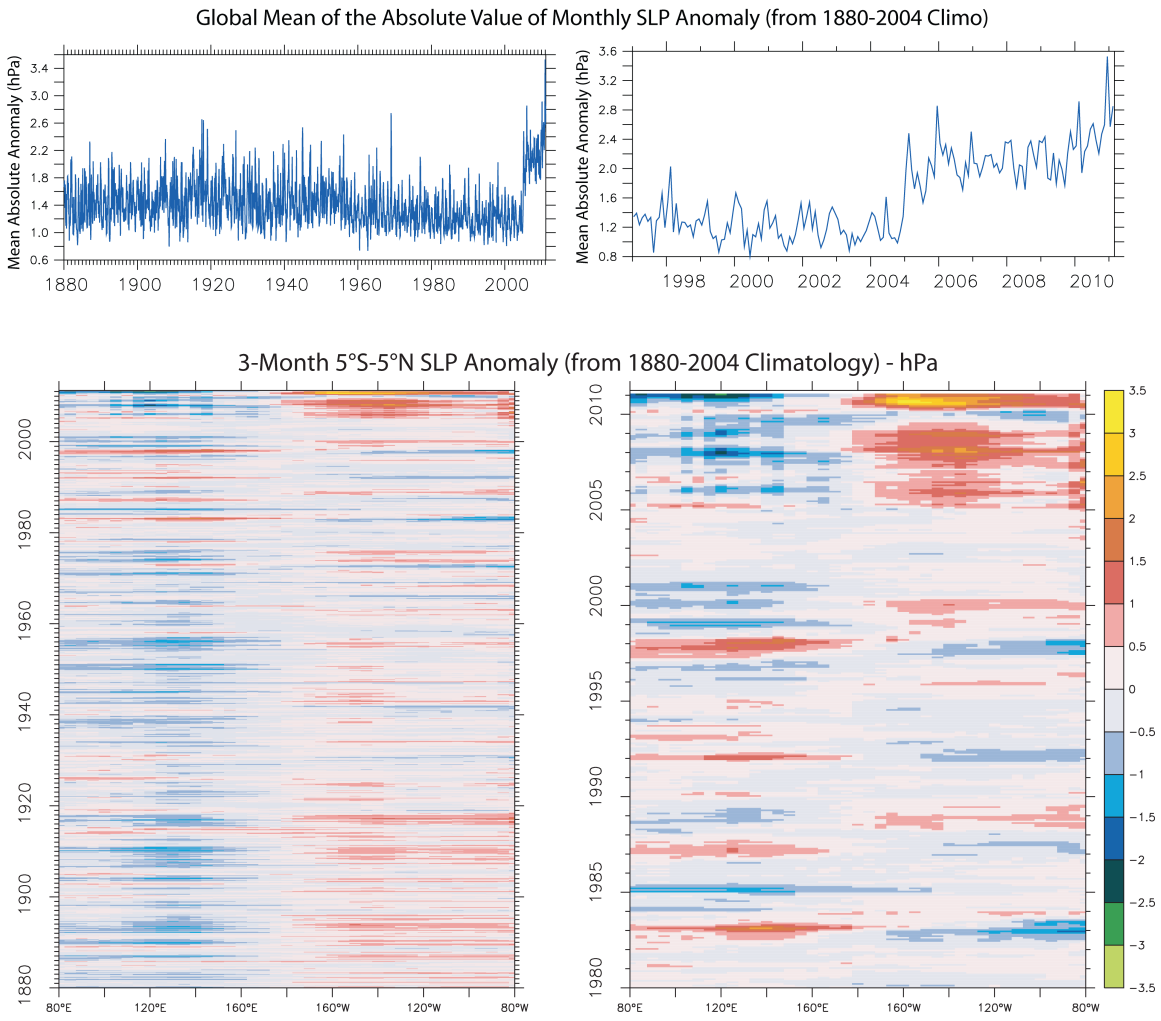

Figure 2 – Impact of the extension of HadSLP2 past 2004 in the HadSLP2r dataset. Upper panels show time-series of the global mean of the absolute value of SLP anomaly (relative to the 1880-2004 average), with the left panel focusing on the end of the record. Notice the change in the amplitude of the typical SLP anomalies coincident with the switch in 2004 between HadSLP2 (Allan and Ansell 2006) and HadSLP2r (real-time updates); the "typical" anomalies are almost twice as large 2005-2011 than prior to that. Lower panels show hovmoller plots of near-equatorial Pacific seasonally smoothed SLP anomaly. Right panel focuses on the end of the record in the left panel. Notice how the anomalies starting in 2005 are unprecedented, exceeding even the extreme La Niña of 1998-9, or the largest El Niños on record (1982-3 and 1997-8).

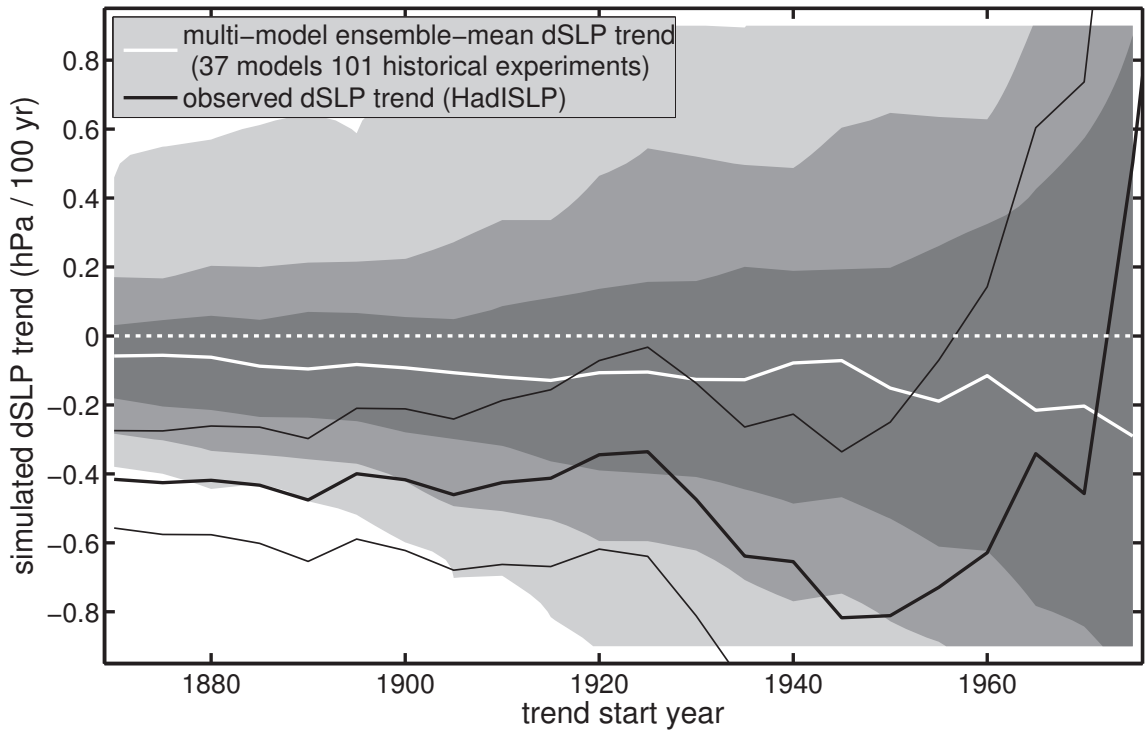

Figure 3 – Probability of the simulated dSLP trends as a function of detection period computed using the ensemble of 104 'historical' experiments. Shading shows the 0.5% (3σ), 2.5% (2σ), 16.5% (1σ) percentile ranges from lighter to darker gray so that the shaded area covers 99%, 95%, and 66% of the trends respectively. See Figure 1 or Section 2 for details on the computation of dSLP index. The detection periods begin at different years from 1870 to 1980 (x-axis) all ending in 2004. The solid white line is the multi-model ensemble-mean trend dSLP trends for each detection period. The solid black line is the observed trend for each detection period. The thin black lines delimit the 1σ confidence interval of the observed trends computed from Student-t distribution with reduced degrees of freedom accounting for auto-correlation in the dSLP index.

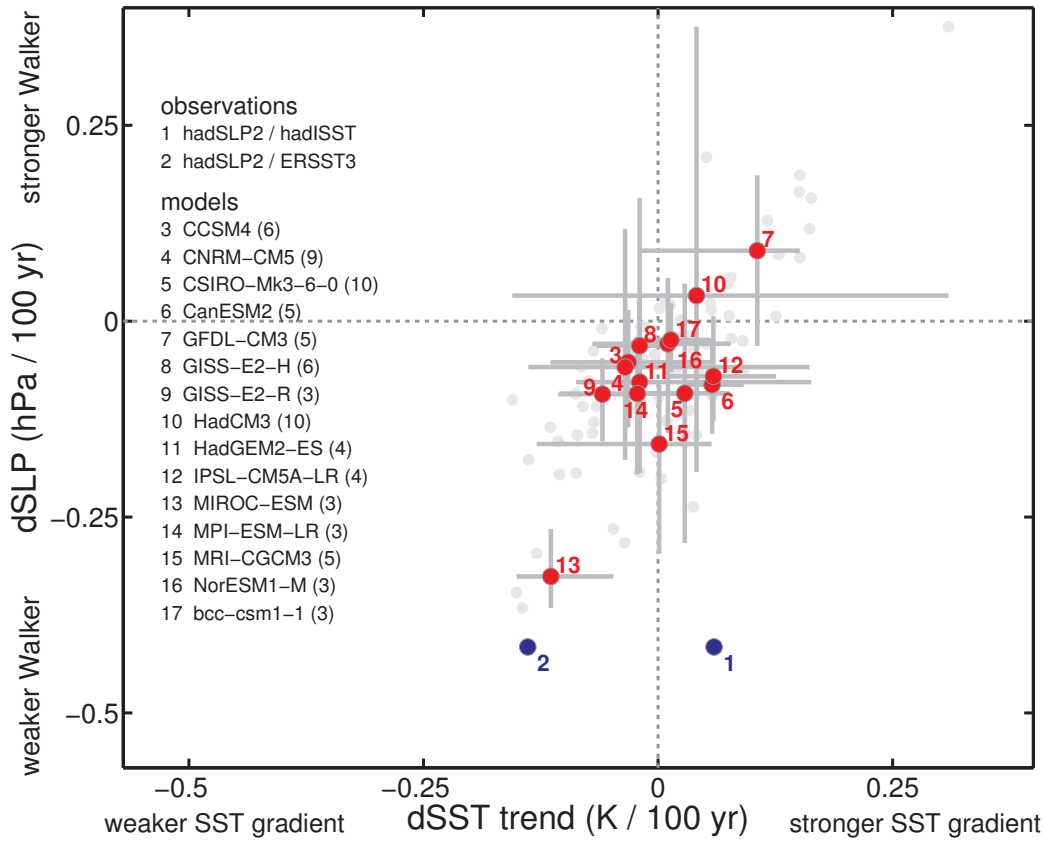

489

490 **Figure 4** – Linear trends in the east-west equatorial gradients of sea surface temperature (dSST) and sea
491 level pressure (dSLP) during the 1870 to 2004 period in observations (blue) and in CMIP5 historical
492 experiments (red). The SLP gradient (dSLP) is a measure of the strength of the Walker circulation. See
493 Figure 1 or Section 2 for details on the dSLP and dSST indeces. The red dots are the ensemble-mean trend
494 for each model and the error bars show the spread among the trends simulated by the model in each
495 experiment. The error bars are the max-min values of the dSLP and dSST trends. The gray dots are the
496 trends from each individual experiment. Only changes simulated by models with more than one historical
497 experiment are shown. The number along with the model name indicates the number of runs of the
498 historical experiment run by each model. The error bars of the observed trends is given by the 1σ
499 confidence interval computed using a Student-t with reduced degrees of freedom to account for auto-
500 correlation in the timeseries.

501

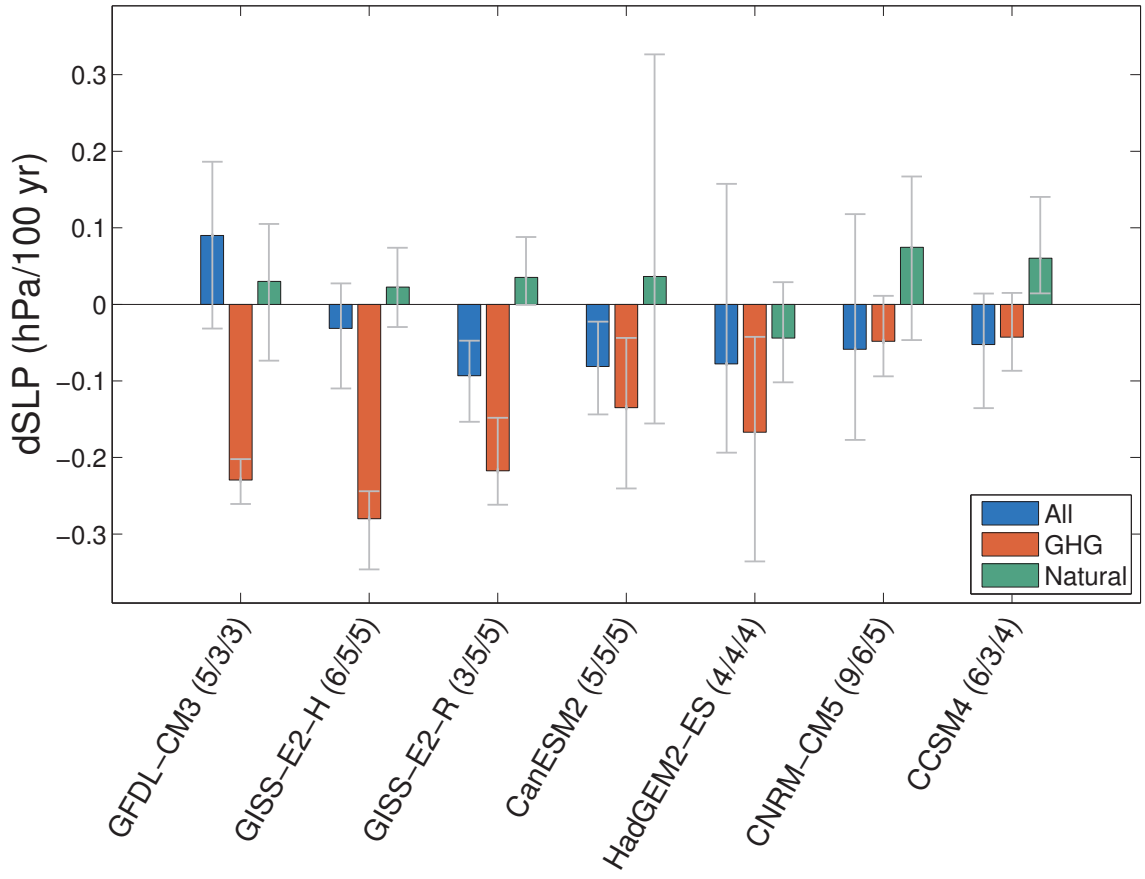

Figure 5 – Linear trends in the east-west sea level pressure gradient (dSLP) during the 1870 to 2004 period simulated by CMIP5 historical (blue), historicalGHG (red), and historicalNat (green) experiments. See Figure 2 for details on how the dSLP index is computed. The bars are the ensemble-mean (EM) trend simulated by each model. The error bars show the min-max range of the trends simulated the different experiments performed with each model. The number along with the model name indicates the number of experiments performed with each model respectively.

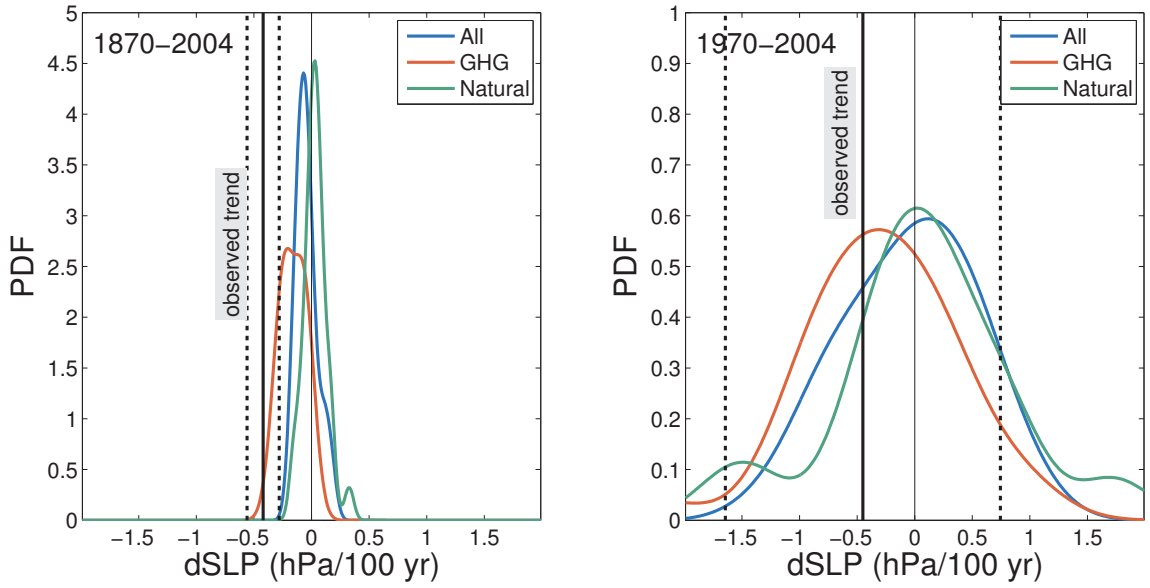

512

513 **Figure 6** – Probability density function of the dSLP trends during (a) 1870-2004 and (b) 1970-2004

514 simulated in historical experiments forced solely with all (blue), anthropogenic greenhouse gas (red) and

515 natural (green) forcings. The solid black line is the observed trend with the dashed lines delimiting the 1σ

516 confidence interval of the observed trends computed from Student-t distribution with reduced degrees of

517 freedom accounting for auto-correlation in the dSLP index.

518

519

520